The EMBO Journal (2007) 26, 4413–4422 | © 2007 European Molecular Biology Organization | All Rights Reserved 0261-4189/07
www.embojournal.org

THE EMBO JOURNAL

Structural analysis of the ParR/*parC* plasmid partition complex

Jakob Møller-Jensen[1,4,*], Simon Ringgaard[2], Christopher P Mercogliano[1], Kenn Gerdes[3] and Jan Löwe[1,*]

[1]MRC-Laboratory of Molecular Biology, Cambridge, UK, [2]Department of Biochemistry and Molecular Biology, University of Southern Denmark, Odense M, Denmark and [3]Institute for Cell and Molecular Biosciences, Newcastle University, Newcastle upon Tyne, UK

Accurate DNA partition at cell division is vital to all living organisms. In bacteria, this process can involve partition loci, which are found on both chromosomes and plasmids. The initial step in *Escherichia coli* plasmid R1 partition involves the formation of a partition complex between the DNA-binding protein ParR and its cognate centromere site *parC* on the DNA. The partition complex is recognized by a second partition protein, the actin-like ATPase ParM, which forms filaments required for the active bidirectional movement of DNA replicates. Here, we present the 2.8 Å crystal structure of ParR from *E. coli* plasmid pB171. ParR forms a tight dimer resembling a large family of dimeric ribbon–helix–helix $(RHH)_2$ site-specific DNA-binding proteins. Crystallographic and electron microscopic data further indicate that ParR dimers assemble into a helix structure with DNA-binding sites facing outward. Genetic and biochemical experiments support a structural arrangement in which the centromere-like *parC* DNA is wrapped around a ParR protein scaffold. This structure holds implications for how ParM polymerization drives active DNA transport during plasmid partition.

The EMBO Journal (2007) **26,** 4413–4422. doi:10.1038/sj.emboj.7601864; Published online 27 September 2007
Subject Categories: cell cycle; structural biology
Keywords: centromere; DNA segregation; ParR; partition complex; plasmid

Introduction

Faithful inheritance of genetic information requires accurate partition of replicated DNA molecules into daughter cell compartments before cell division. Akin to mitosis in eukaryotes the process of DNA partition in prokaryotes is a highly dynamic process in which the DNA replicates are separated and transported to opposite sides of the cell division plane (Gerdes *et al*, 2004). To a large extent, our knowledge about DNA partition in bacteria is derived from studies of how low-copy-number plasmids are segregated. Such plasmids rely exclusively on partition loci (*par*) for their specific distribution to progeny in every cell cycle. In addition, partition loci have been identified on a large number of bacterial chromosomes and appear to play an important role in the spatial organization of chromosomal DNA as well (Gerdes *et al*, 2000; Yamaichi and Niki, 2000; Hayes, 2000; Wu and Errington, 2003; Errington *et al*, 2005; Fogel and Waldor, 2006; Lee and Grossman, 2006; Yamaichi *et al*, 2007). Partition systems are generally composed of three essential elements, all specified by the same genetic locus: two proteins, an ATPase and a DNA-binding adaptor protein, that act together on a *cis*-acting centromere-like region on the DNA. When classified according to the nature of their ATPase component, partition systems fall into two main categories: type I systems that employ Walker-type ATPases termed ParA, ParF or SopA, and type II systems whose ATPases, termed ParM, are homologs of actin. Type I partition systems further fall into two subgroups type Ia and type Ib based on the size of the Walker ATPases. The adaptor proteins of type Ia, type Ib and type II partition systems (termed ParB, ParG and ParR, respectively) show no homology even though they have similar functions in the partition process, and the centromere-like sites they recognize are diverse (Gerdes *et al*, 2000; Hayes, 2000).

The earliest step in a general mechanistic outline of plasmid partition involves the formation of a partition complex between the adaptor protein and its cognate centromere-like site on the DNA. In *parMRC* from plasmid R1, which is typical of partitioning systems with actin-like ATPases (type II), the dimeric ParR adaptor protein, which is present in less than 1000 copies in the cell (Møller-Jensen *et al*, 2002), binds cooperatively to two sets of five 11-bp direct repeats denoted *parC* (Dam and Gerdes, 1994; Møller-Jensen *et al*, 2003). The *parC* DNA region has been shown to be intrinsically curved (Hoischen *et al*, 2004). Apart from its function in plasmid partition, ParR binding serves to autoregulate the expression of partition proteins as the *parC* site overlaps with the *par*-promoter (Jensen *et al*, 1994). A minimum of two direct repeats of DNA is required for binding of ParR and footprinting analysis have shown that the partition complex extends over the entire *parC* region (Møller-Jensen *et al*, 2003). Formation of the ParR/*parC* DNA partition complex has been shown by electron microscopy to mediate pairing of plasmid replicates (Jensen *et al*, 1998).

In the *parABS* system of plasmid P1, which employs a Walker type ATPase (type Ia), the partition complex is formed by association of a ParB dimer and the host-encoded Integration Host Factor with specific recognition sequences in the centromeric DNA region, *parS* (Bouet *et al*, 2000). Formation of the partition complex is thought to mediate specific pairing of plasmid replicates at *parS* sites (Edgar *et al*, 2001). A recent

*Corresponding authors. J Møller-Jensen, Department of Biochemistry and Molecular Biology, University of Southern Denmark, Campusvej 55, Odense M 5230, Denmark. Tel.: +45 6550 2423; Fax: +45 6550 2467; E-mail: jakobm@bmb.sdu.dk or J Löwe, MRC-Laboratory of Molecular Biology, Hills Road, Cambridge CB2 0QH, UK. Tel.: +44 1223 252969; Fax: +44 1223 213556; E-mail: jyl@mrc-lmb.cam.ac.uk
[4]Present address: Department of Biochemistry and Molecular Biology, University of Southern Denmark, Campusvej 55, Odense M 5230, Denmark

Received: 9 February 2007; accepted: 31 August 2007; published online: 27 September 2007

crystal structure of ParB bound to DNA provided mechanistic insight into how ParB-mediated plasmid pairing might occur by demonstrating that ParB dimers bound to DNA via their N-terminal helix–turn–helix (HTH) domain could associate *in trans* with a different DNA molecule via their dimerization domain and thus serve as a molecular linkage between two plasmid centromers (Schumacher and Funnell, 2005).

The partition complexes are recognized by partition ATPases that convert energy from ATP hydrolysis into active intracellular transport of plasmid molecules. Both ParA and ParM type ATPases have been shown to form filamentous structures, although ATP-dependent dynamics remain to be demonstrated for ParA proteins (Møller-Jensen *et al*, 2002, 2003; Barilla *et al*, 2005; Leonard *et al*, 2005; Lim *et al*, 2005; Becker *et al*, 2006; Ebersbach *et al*, 2006; Bouet *et al*, 2007). *In vitro* ParM filaments nucleate spontaneously in the presence of ATP and extend bidirectionally. In the absence of ParR and *parC* DNA, the ParM filament growth phase is succeeded by rapid unidirectional collapse, a phenomenon reminiscent of the dynamic instability displayed by microtubules in eukaryotes (Garner *et al*, 2004). In a recent study, active DNA segregation was reconstituted from purified ParM, ParR and *parC* DNA components, indicating that these essential components are sufficient to form a bipolar, plasmid-segregating spindle (Garner *et al*, 2007). ParR/*parC* complexes interacted with both ends of the ParM filaments in the reconstituted plasmid segregation assay thereby stabilizing them against depolymerization, while allowing for insertion of new ParM monomers at the filament tip (Garner *et al*, 2007). This finding is consistent with previously proposed insertional polymerization models for plasmid movement (Møller-Jensen *et al*, 2003; Garner *et al*, 2004).

An important question concerns the overall architecture of partition complexes and how they interact with the force-generating ATPases during the DNA partition process. In this work, we present the crystal structure of the adaptor protein ParR from plasmid pB171. This protein binds to the *parC1* centromere-like region of the double partition locus of *Escherichia coli* pB171 (Ebersbach and Gerdes, 2001) and the binding site is characterized by two identical 10-bp high-affinity sequences separated by 31 bp (Ringgaard *et al*, 2007). ParR forms a tight dimer, which further assembles into a ring or helix structure with putative DNA-binding regions facing outward. The position of the DNA-binding domain is confirmed by introduction of site-specific amino-acid substitutions on ParR, followed by functional analysis *in vivo* and *in vitro*. Electron microscopic examination of ParR/*parC* DNA complexes further reveal the formation of ParR rings, suggesting that the crystalline packing of ParR protein into a helix is physiologically relevant. This partition complex architecture leads us to propose a model for active plasmid movement in which ParR protein encircle or bind to growing ParM filament tips either as a helix or a ring through interactions involving the ParR C-terminus, while *parC* DNA is wrapped on the outside through interactions with the ParR N-terminus.

Results

ParR forms ring-like structures on parC DNA

In a previous study, plasmid R1 ParR was shown by electron microscopy (EM) to bind to plasmid *parC* regions and mediate site-specific pairing of DNA molecules (Jensen *et al*, 1998). Here, we further examine the ParR/*parC* DNA partition complex structure using improved staining techniques for EM imaging. Specifically, we have omitted the use of aldehyde fixatives before negative staining. We now demonstrate that plasmid R1 ParR forms ring-shaped complexes on pre-linearized DNA containing *parC* regions. Images of ParR/*parC* DNA complexes shown in Figure 1 were obtained by rotary shadowing (panels B–J) and negative staining (panels K–R). Figure 1O–R shows enlarged images of negatively stained ParR rings on DNA. Ring structures always formed at the *parC* site as judged from the conserved distance to the *Sca*I restriction site and they never formed on control DNA without the *parC* region or in the absence of DNA (data not shown). Also, no ring structures were observed on *parC* DNA in the absence of ParR protein (Figure 1A). The ParR rings measured between 15 and 20 nm in diameter, which is consistent with the 15 nm ParR helix diameter shown in Figure 2A plus the DNA wrapped around it. Figure 1I and J shows examples of DNA pairing by close association of ParR rings.

ParR belongs to the MetJ/Arc superfamily of DNA binding proteins

Attempts to determine the structure of plasmid R1 ParR by X-ray crystallography proved unsuccessful as the protein formed needle-shaped crystals of insufficient size and quality for structure determination. Instead, we have determined the structure of the homologous ParR from *E. coli* plasmid pB171. This protein has 25% sequence identity and 44% similarity over all residues to plasmid R1 ParR (Figure 3). The structure contains two monomers in the asymmetric unit, each consisting of a short N-terminal β-strand, followed by four or five α-helices (Figure 2A). The two monomers of the asymmetric unit are related by a pseudo-two-fold axis and form a tight antiparallel homodimer in which one monomer is distinguishable by a short α-helix H5 near the C-terminus. The polypeptide chains were traceable in the electron density from Lys6 to Leu95, leaving the C-terminal 35 amino acids disordered. The dimer N-termini form a ribbon–helix–helix $(RHH)_2$ structure in which a short two-stranded antiparallel β-ribbon (S1) is flanked by two sets of α-helices (H1 and H2). The compact RHH_2 motif, which is held together by a core of hydrophobic interactions, is followed by short α-helices (H3–H5). The side and top view of a ParR dimer structure is shown in Figure 2A. The family of bacterial RHH_2 proteins is typified by the MetJ and Arc transcriptional repressors, both of which have been crystallized in complex with their respective operator DNA (Somers and Phillips, 1992; Raumann *et al*, 1994b). These proteins contain a two-stranded antiparallel β-ribbon structure that interacts with base-determinants in the DNA major groove. This interaction is stabilized by interactions between the DNA backbone phosphates and α-helices H1 and H2 (Raumann *et al*, 1994a). Other members of this protein family include CopG, a repressor involved in plasmid copy-number-control (Gomis-Ruth *et al*, 1998), and the plasmid-encoded partition adaptor proteins ParG (Golovanov *et al*, 2003) and Omega (Weihofen *et al*, 2006), the structures of which are shown in Figure 2C.

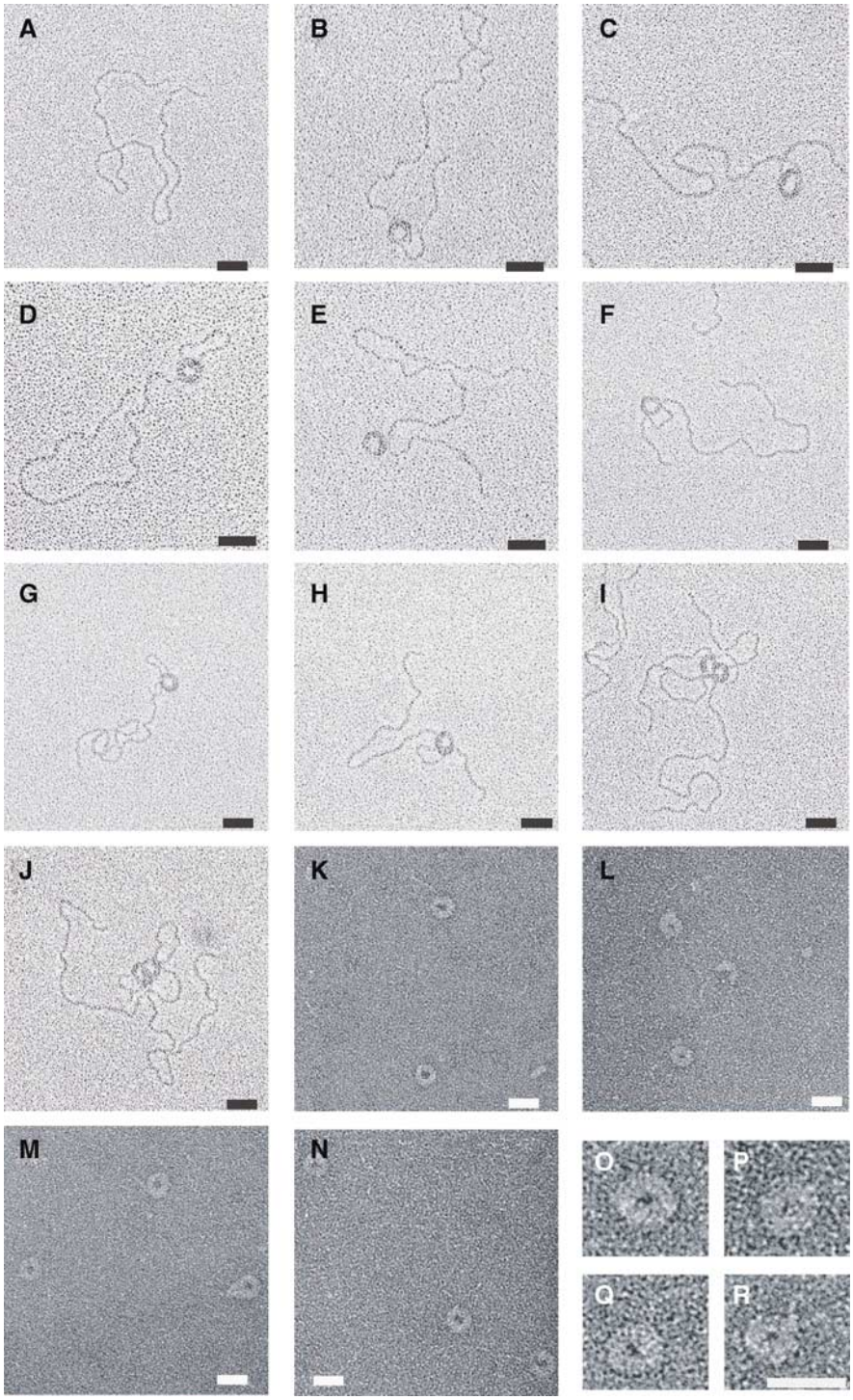

Figure 1 EM visualization of ParR/*parC* DNA partition complexes. Electron micrographs of ParR incubated with *parC* DNA. (**A**) No added ParR. (**B**–**J**) Complexes between ParR and linearized pMD330 stained by rotary shadowing. (**K**–**R**) Negatively stained complexes of ParR and a 383 bp *parC* PCR product. ParR forms ring-shaped complexes on *parC*-containing DNA and close association of rings mediate DNA pairing (I, J). Size bars correspond to 25 nm.

ParR dimers multimerize to form a helical DNA-binding scaffold

A unifying feature of RHH_2 proteins is the cooperative nature of their DNA binding. In all cases, the minimum binding entity is comprised by a dimer of dimers and the complexes are stabilized by cooperative interdimer contacts. In our ParR crystal lattice, the proteins assemble into a continuous helix structure consisting of 12 ParR dimers per full 360° turn. ParR dimers are arranged with their N-termini facing outward and their C-termini pointing towards the helix center. As shown in Figure 2B, a helical turn along the screw axis results in a translation of 13 nm. The view along the screw axis demonstrates that the ParR helix has a diameter of 15 nm and is made up from six symmetrical pairs of dimers such that every ParR dimer is related to its nearest neighbor by a 30° rotation and a two-fold symmetry axis. The dimers are held together

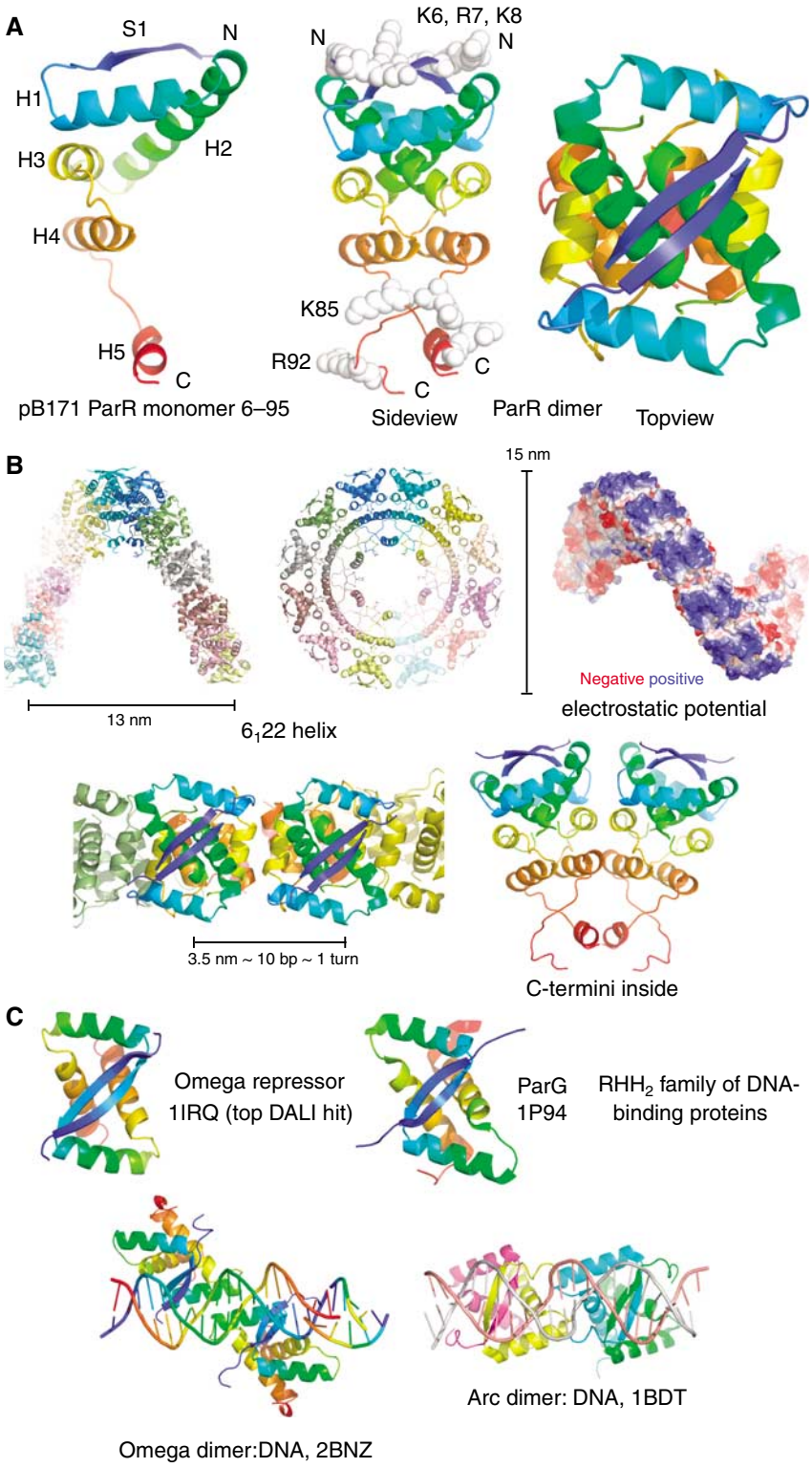

Figure 2 Crystal structure of ParR. (**A**) Crystal structure of ParR from pB171. The monomer (left) contains an N-terminal β-strand S1 followed by α-helices H1–H5. The protein crystallizes as a tight dimer with an N-terminal ribbon–helix–helix domain as seen from the side (middle) and top (right). Amino acids subjected to mutagenesis are highlighted as white spheres. (**B**) ParR assembles into a helix with a 13 nm translation per turn (top left) and a 15 nm diameter when viewed along the screw axis (top center). RHH_2 domains form regularly spaced basic patches on the helix exterior (top right) and the distance between adjacent β-ribbon structures corresponds to one helical turn of DNA double helix (bottom left). Dimers are related reciprocally in the helix mostly through interactions between residues in helices H3, H4 and H5 (bottom right). (**C**) Structures of the RHH_2 domain from the homologous Omega and ParG proteins (top) highlight their close structural similarity despite the absence of detectable sequence similarity, even after structure-based alignments. Bottom: crystal structures of Omega and Arc proteins in complex with their respective operator DNA. The proteins insert antiparallel β-strands into the DNA major groove and the dimers then assemble into higher order assemblies that are quite different from each other. In ParR, this domain is positioned on the outside of the helix (B). The different quaternary interactions reflect the diverse arrangements of the cognate DNA motifs and produce different complexes when more proteins are added, sometimes spreading beyond the site-specific binding region in the DNA.

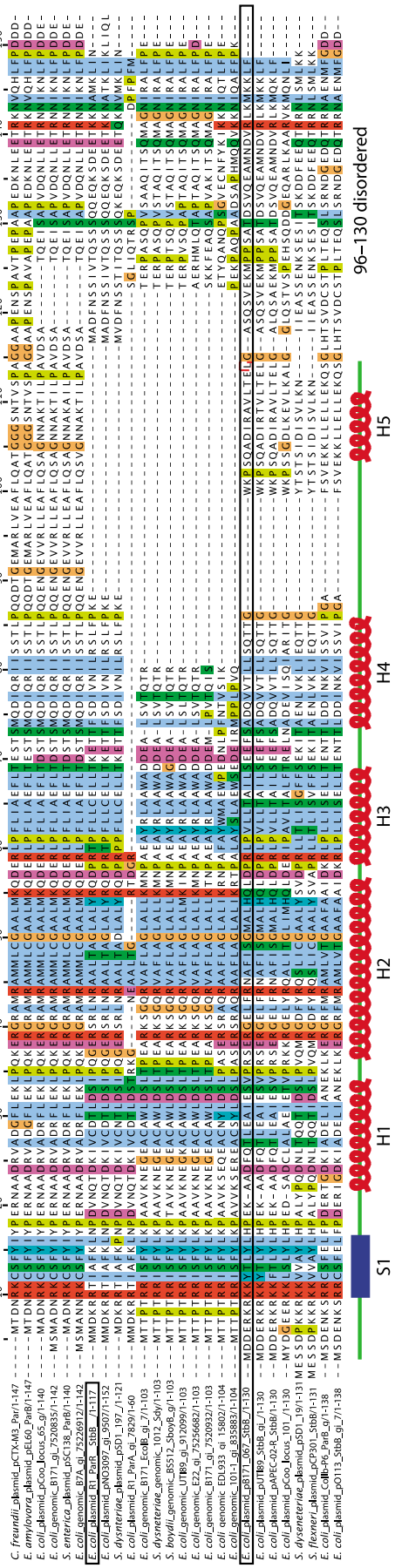

mostly by interactions between amino-acid side chains in H3, H4 and H5. The N-terminal RHH_2 domains align on the helix exterior and form regularly spaced basic patches as can be seen in the surface potential representation in Figure 2B. The fact that the RHH_2 DNA-binding sites are positioned 3.5 nm apart, which corresponds almost exactly to one helical turn of B-helix DNA and is in register with the repeat structure of the *parC1* centromere-like site, strongly advocates a physiological relevance of the crystalline packing of ParR. Thus, the crystal structure suggests a partition complex architecture in which the centromere-like *parC1* region wraps around a helical scaffold formed by ParR protein.

The ParR fold is conserved

A multiple sequence alignment of chromosomal and plasmid-encoded ParR homologs from *E. coli* and other closely related gamma proteobacteria is shown in Figure 3. The aligned sequences display a large degree of sequence conservation in the N-terminal RHH_2 domain, as well as in helix H3 and H4, which are involved in interdimer contacts. This alignment includes ParR from R1, which is the prototypical type II partition system and is used for our EM studies. RHH_2 secondary structure elements are succeeded by conserved proline residues that induce sharp bends in the polypeptide chain responsible for the wedge shape of the molecule. The aligned sequences differ in the H5 region, where certain proteins contain insertions. Interestingly, the C-terminus, which is disordered in our ParR crystal structure, shows high sequence conservation, indicating that this part of the protein may be important for the partition function.

The RHH_2 motif is required for DNA binding and plasmid partition

To verify that the DNA-binding interface of ParR of pB171 is in fact the N-terminal RHH_2 domain, we carried out site-specific mutagenesis of residues Lys6, Arg7 and Lys8, which are presumed to be involved in contact with the DNA. As negative control, we performed amino-acid substitutions closer to the C-terminus at Lys85 and Arg92. Lysine residues were mutated into glutamic acid and arginines were substituted by Serine. The position of the mutated amino-acid residues is shown in Figure 2A in white space fill representation. Mutant *parR* genes were tested for functionality in their natural genetic context on test plasmids derived from low-copy-number plasmid pGE103, which contains the wild-type (wt) partition locus from pB171 (Ebersbach and Gerdes,

Figure 3 Structure-based sequence alignment of chromosomal and plasmid-encoded ParR homologs from enterobacteria. The aligned genomic and plasmid sequences are retrieved from the closely related enterobacteria *Citrobacter*, *Erwinia*, *Shigella* ssp., *Salmonella* and *E. coli*. No additional ParR-related sequences are currently detectable in the databases using phi-BLAST searches. Conserved arginine and lysine residues are colored red and conserved nonpolar residues of α-helices are colored in blue. The conserved proline residues that bend the polypeptide chain are highlighted in green. The sequence of the crystallized ParR from pB171 is boxed and the secondary structure elements, as derived from our structure of pB171 ParR, are indicated in cartoon below the aligned sequences. The ParR protein from plasmid R1 is highlighted by a second box. The structure determined here (Figure 2) describes the large N-terminal domain conserved amongst all the proteins. An additional domain, disordered in our crystals and therefore mobile or unstructured can be found at the C-terminus of all proteins. The alignment was done using ClustalW.

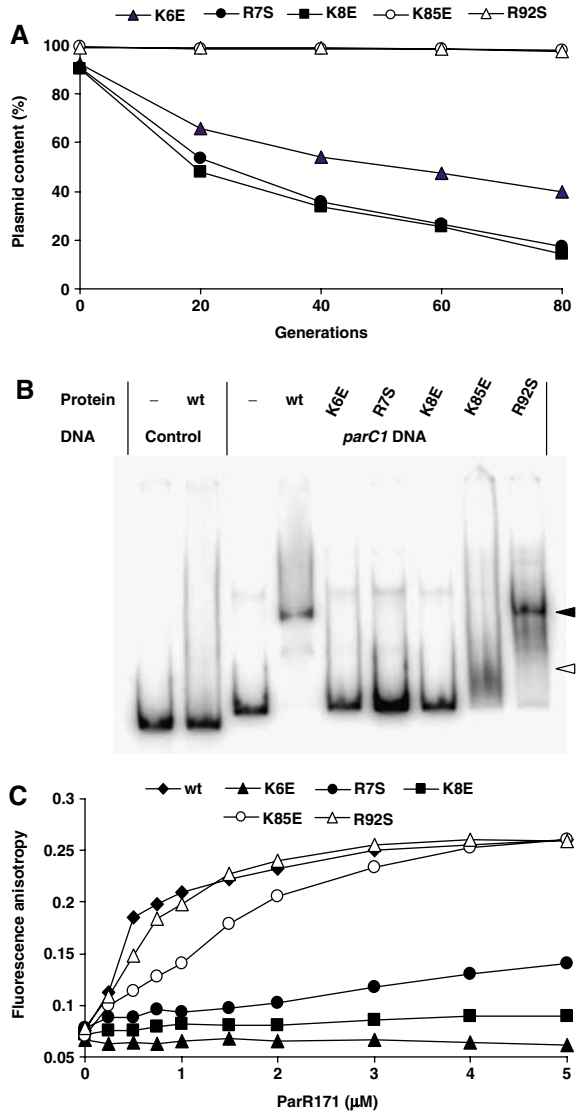

Figure 4 The ParR RHH_2 domain is required for *parC* DNA binding and plasmid partition. (**A**) Determination of partition function in plasmids containing mutated *parR171* genes. The fraction of plasmid-containing cells is plotted as a function of the number generations of nonselective growth. (▲) pJMJ206, ParR171-K6E mutation; (●) pJMJ207, ParR171-R7S mutation; (■) pJMJ208, ParR171-K8E mutation; (○) pJMJ285, ParR171-K85E mutation; (△) pJMJ292, ParR171-R92S mutation. (**B**) Gelshift assay of wild-type (wt) and mutant ParR binding to DNA. A 2 nM volume of *parC1* or nonspecific control DNA was incubated in the absence (–) or presence of 2 μM wt or mutant ParR. Full binding by wt and R92S-mutated ParR to the *parC1* DNA site is indicated by the black arrowhead, whereas partial binding by ParR-K85E is indicated by a white arrowhead. (**C**) Analysis of wt and mutant ParR171 binding to *parC1* by fluorescence anisotropy. (♦) Wt ParR171; (▲) ParR171-K6E; (●) ParR171-R7S; (■) ParR171-K8E; (○) ParR171-K85E; (△) ParR171-R92S.

2001). For the plasmid stabilization assay, cells were grown in nonselective medium and the fraction of plasmid-containing cells was determined by plating on nonselective indicator plates containing X-gal. As shown in Figure 4A, test plasmids containing the ParR171 K6E, R7S and K8E mutations severely impaired the function of ParR171. By contrast, ParR171 K85E and R92S mutations seemed to have no effect on *par* activity as the plasmids were stably maintained throughout the assay. To correlate the observed deficiency of N-terminal mutants in ParR171 with lack of DNA binding, we purified mutant versions of ParR and tested these for binding to *parC1* DNA by gelshift analysis and fluorescence anisotropy measurements (Figure 4B and C). As reported previously, wt ParR from pB171 associates specifically with *parC1* DNA (Figure 4B, lanes 1–4) (Ringgaard *et al*, 2007). No retardation was observed with a nonspecific control DNA fragment. The introduction of K6E, R7S and K8E mutations abolished the ability of ParR to bind to *parC1* DNA, whereas ParR with K85E and R92S mutations could still bind to the DNA (Figure 4, lanes 5–9). These findings are supported by fluorescence anisotropy measurements showing impaired DNA binding of the K6E, R7S and K8E mutant proteins and retained binding capacity of the K85E and R92S mutant proteins. The fact that K85E-mutated ParR did only display partial retardation in the gelshift could be explained by a disruptive effect of this amino-acid substitution on dimer–dimer interaction such that spreading beyond high-affinity sites is limited (white arrow head). This assumption is corroborated by the fluorescence anisotropy data showing reduced binding cooperativity of this mutant protein. In conclusion, these results demonstrate that the N-terminal RHH_2 domain is required for DNA binding and that disruption of the interactions to *parC1* DNA leads to impaired plasmid partition.

Discussion

RHH_2 structures: variations on the same theme

Members of the MetJ/Arc protein superfamily include the plasmid-encoded repressors Omega (Weihofen *et al*, 2006), CopG (Gomis-Ruth *et al*, 1998), ParG (Golovanov *et al*, 2003) and ParR. All share the same DNA-binding RHH_2 motif and their mode of DNA recognition is similar. The binding specificity is determined by interactions between side chains of the antiparallel β-ribbon and bases in the DNA major groove. This interaction is further stabilized by interactions formed between the DNA phosphate backbone and side chains of helix H1 and main chain amines of helix H2, respectively. In most cases, the RHH_2 domain is located at or near the N-terminus, but it can also be located C-terminally, as in the case of ParG shown in Figure 2C (Golovanov *et al*, 2003). Our crystal structure of ParR from pB171 showed the presence of an N-terminal RHH_2 domain. Although attempts to co-crystallize ParR with *parC1* DNA proved unsuccessful, we confirmed the involvement of this domain in DNA recognition and plasmid partition by genetic and biochemical data shown in Figure 4.

Although RHH_2 proteins generally exist as dimers in solution, they bind to DNA in a cooperative fashion and form tetramers or higher order oligomers through quaternary dimer–dimer (protein–protein) interactions. These quaternary relationships are quite diverse and reflect the different compositions of their binding sites on the DNA. Thus, protein–DNA complexes formed by this family display a large degree of structural diversity as illustrated by the structures of Omega (Weihofen *et al*, 2006) and Arc (Raumann *et al*, 1994b) in complex with their respective DNA operators in Figure 2C. Omega dimers bound to adjacent heptad DNA sequences interact through hydrophobic side chains in helix H1, forming a left-handed matrix around straight DNA in which each dimer is related to its neighbor

by a 7-bp translation and a 252° rotation (Weihofen *et al*, 2006). By contrast, two Arc dimers bound to a 21-bp operator site interact using the loop between helices H1 and H2 to form a tetramer that binds on one face of the double helix, thereby inducing a 50° bend in the DNA (Raumann *et al*, 1994b). Thus, binding site length and spacing between adjacent binding sites are important parameters in determining how RHH_2 domains interact on the DNA. Although the RHH_2 domain structure is essentially conserved in proteins of this family, they use it in different ways and for different purposes.

ParR is a bifunctional protein, which acts both as a transcriptional repressor and a partition protein. It blocks transcription from the *par* promoter by binding cooperatively to the iterated recognition sequences in *parC* of plasmid R1 (Dam and Gerdes, 1994; Ringgaard *et al*, 2007) and by arranging the repressor/operator complex further into a specialized hyperstructure that is capable of interacting with polymerizing ParM, ParR functions in plasmid partition as well. In ParR, hydrophobic residues in helices H3, H4 and H5 form extensive dimer–dimer interactions, which shape the scaffold. According to the crystal structure, pB171 ParR will bind on one face of the *parC1* DNA and thereby induce a 30° bend in the DNA per dimer. This is in accordance with the 31 bp (or three helical turns of double helix) spacing of the two high-affinity binding sites in the *parC1* centromere-like region (Ringgaard *et al*, 2007).

ParR packed as a continuous helix in the crystals, but appeared as a ring structure in the EM projections. The screw axis in the crystal may be caused by packing restraints on the one hand, but on the other hand, a ParR helix structure could also be compressed into a closed ring upon application to EM grids. Thus, the EM pictures are projections possibly hiding the helical nature of the ParR arcs. Yet another possibility could be that ParR from plasmids pB171 and R1 form different superstructures. We find this unlikely, however, given the close homology between the two proteins. Despite considerable effort, we were unable to produce negatively stained complexes between ParR171 and DNA for electron microscopic visualization in the absence of aldehyde fixatives, thus making it impossible to discern whether this protein formed ring-shaped complexes (data not shown). Based on the present data, it is not possible to distinguish between ring and helix structures and both would function in the proposed mechanism of plasmid partition. The diameter of a closed ParR ring structure would perhaps be too small to encircle the ParM filament. A comparison of the ParM filament cross-section and the ParR scaffold diameter is shown in Figure 5B. Another point arguing in favor of a helical ParR scaffold is the fact that wrapping of DNA around a disc-shaped scaffold would result in a steric clash between DNA entering and exiting the complex.

Implications for the plasmid partition mechanism

Previous studies of the partition system from plasmid R1 have provided detailed information about the mechanism of active plasmid distribution in the cell. Pairing of replicated plasmids by formation of the ParR/*parC* complex leads to the formation of dynamic ParM filaments that push the plasmid copies apart at the expense of ATP hydrolysis (Møller-Jensen *et al*, 2002, 2003). The ParM filament structure is similar to F-actin and employs essentially the same mechanism of ATP-driven polymerization as actin (van den Ent *et al*, 2002). In the absence of ParR and *parC* DNA, ParM filaments were found to be extremely dynamic and transient, switching between stages of bidirectional growth and shortening (Garner *et al*, 2004). This dynamic instability of ParM filaments led to the proposal that bidirectional plasmid transport could involve capping of both filament ends by ParR/*parC* complexes, which stabilize the growing ParM filament (Garner *et al*, 2004). Bipolar stabilization of ParM filaments by ParR/*parC* complexes has been shown directly in a reconstituted DNA motility assay, which demonstrated the rapid decay of ParM polymers with uncapped tips (Garner *et al*, 2007). These findings are consistent with immunofluorescence-imaging of *E. coli* cells demonstrating that plasmids

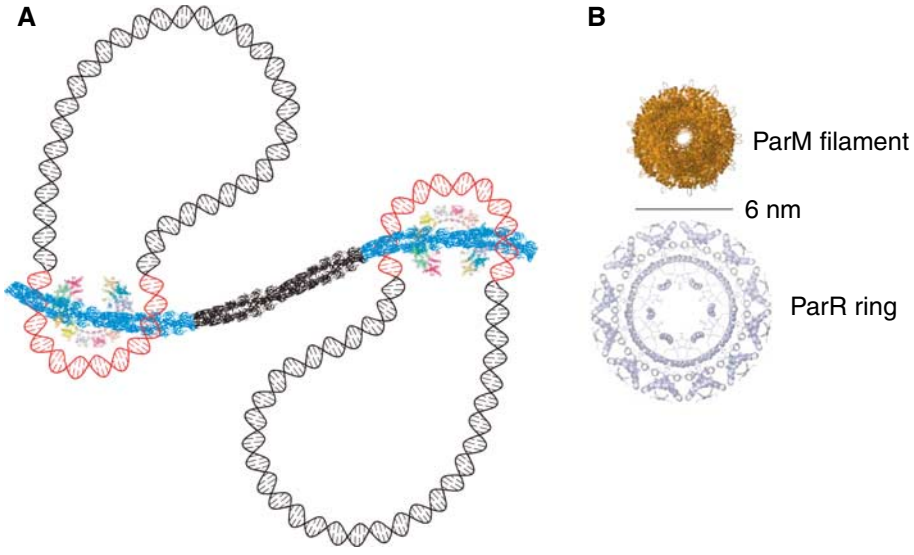

Figure 5 Model of R1 plasmid segregation. (**A**) Cartoon showing how ParR/*parC* DNA complexes interact with opposite ends of a growing ParM filament. The ParR N-terminal RHH_2 domain binds specifically to *parC* DNA (red) and the ParR C-terminus interacts with ParM-ATP (blue) at or near the filament tips. ATP hydrolysis is proposed to induce a structural rearrangement in ParM that leads to dislodging of ParR, which in turn can reassociate further along the filament. (**B**) Cross-section of the ParM filament and the ParR helical scaffold viewed along the six-fold symmetry axis.

are indeed localized at the filament ends during partition (Møller-Jensen *et al*, 2003).

The structure of the ParR/*parC* partition complex presented here immediately suggests how the ParR protein scaffold can serve as a link between plasmid DNA and the dynamic ParM filament during active transport in the cell. We propose that ParR interacts with ParM through its C-terminus located in the helix or ring interior and thus encircle a growing ParM filament, while contacting the plasmid DNA with the helix/ring exterior. As the ring is quite small, it might also be possible that the ring or arc of ParR binds via the C-termini to the side of the filaments. Figure 5A shows a model of ParM-mediated plasmid partition that takes the new ParR structure into account. In Figure 5B, the ParM filament and ParR helix cross-sections are shown for comparison. With a diameter of about 6 nm, the ParM filament would fit inside the inner ring formed by ParR alpha-helix 3. This arrangement would require the flexible C-terminal part to give way. Alternatively, the helix may open up to accommodate the ParM filament as shown in Figure 5A or it might just bind to the side of the filament. Due to the ParR dimer symmetry, the partition complex is identical in both orientations on the filament and hence will be able to interact with both ends of the polar ParM filament, where ParM monomers exist in the ATP-bound form. If the binding affinity of ParR for ParM-ATP exceeds that for ParM-ADP, this would explain how continuous sliding of partition complexes toward growing filament ends with ATP-bound ParM could take place. An important part of this model is that the energy of ParM ATP hydrolysis would be used for displacing the C-termini from the ADP-containing filament, so that they can re-bind the ATP caps, effectively driving ParR binding along the filament like a motor. Having many ParM-binding sites on the ParR superstructure makes this movement more processive, so ParR (and hence the plasmids) stick to the filament ends at all times.

Materials and methods

Stains and plasmids

E. coli strain DH5α (Invitrogen) was used for cloning and plasmid stability assays. *E. coli* strain BL21AI (Invitrogen) was used for arabinose-induced protein overexpression from T7 promoters. Genes encoding R1 ParR (GI:134956) and pB171 ParR (GI:6009443) were cloned in vector pHis17 (without any additional residues) (van den Ent and Löwe, 2000) resulting in plasmids pJMJ100 and pJMJ101, respectively. Expression plasmids pJMJ106, pJMJ107, pJMJ108, pJMJ185, pJMJ192 were derived from pJMJ101 by PCR mutagenesis. R1 test plasmids pJMJ206, pJMJ207, pJMJ208, pJMJ285, pJMJ292 were derived from pGE103, which contains a functional *par1* locus from *E. coli* pB171 (Ebersbach and Gerdes, 2001) by PCR mutagenesis.

Protein expression and purification

R1 ParR and pB171 ParR proteins were overexpressed in *E. coli* BL21-AI cells (Invitrogen). Cells were grown at 37°C in 2× TY medium supplemented with 100 μg/ml ampicillin and 0.2% glucose. At mid-exponential growth, protein expression was induced by addition of 0.4% arabinose. After 6 h of induction, the cells were harvested, resuspended in buffer A (50 mM Tris–HCl, pH 7; 100 mM KCl; 1 mM EDTA; 1 mM DTT) containing 5 μg/ml DNaseI and 1 mg/ml lysozyme, and lysed by sonication. The lysate was cleared by centrifugation for 45 min at 100 000 *g*. The cleared lysate was then loaded on a 5 ml HiTrap (GE Healthcare) heparin column and protein was eluted with a linear gradient of buffer B (buffer A + 1 M NaCl). Fractions containing partially pure protein were pooled, diluted 100-fold in Buffer A and loaded onto a 5 ml HiTrap SP HP cation exchange column. Again, protein was eluted with a linear gradient of buffer B. Purified protein was gel filtrated in buffer C (20 mM Tris–HCl pH 9; 50 mM KCl; 1 mM EDTA; 1 mM NaN_3), concentrated to 10 mg/ml and snap-frozen in liquid nitrogen. Purified R1 ParR and pB171 ParR tend to precipitate reversibly at pH below 8.5. The correct identity of the purified protein was verified by electrospray ionization mass spectrometry. The typical yields exceeded 10 mg protein per liter culture.

For purification of mutant pB171 ParR proteins, the pB171 *parR* reading frame was cloned into pOP-TM (gift from Olga Perisic) to create an in-frame MBP-ParR gene fusion containing a TEV cleavage site between the two protein moieties. Site-specific amino-acid substitutions were introduced by PCR. TEV cleavage leaves a glycine-serine-histidine residual at the pB171 ParR amino terminus. MBP-ParR was overexpressed using BL21-AI as described above. The cells were lysed in buffer D (50 mM Tris–HCl pH 7.5; 500 mM NaCl; 1 mM EDTA; 1 mM DTT) containing 5 μg/ml DNaseI and 1 mg/ml lysozyme and lysed by sonication. Cleared lysates were loaded onto amylose resin (New England Biolabs), washed in buffer D and eluted by addition of 15 mM maltose in buffer D. Purified fusion protein was dialyzed into buffer E (50 mM Tris–HCl, pH 8.8; 25 mM KCl; 1 mM EDTA; 1 mM DTT) and incubated with TEV protease for 4 h at room temperature. The cleavage products were separated on a HiTrap Q HP ion exchange column using a linear gradient from 25 mM to 1 M NaCl in buffer E. All mutant proteins behaved similarly during purification and displayed similar column elution profiles, indicating that overall protein folding was not affected by the amino-acid substitutions. Fractions containing pure mutant pB171 ParR protein were pooled dialyzed into buffer E, concentrated and frozen.

Crystallization, data collection and structure determination

Initial crystallization conditions were found using our in-house 100 nl high-throughput crystallization screen of 1500 standard conditions (Stock *et al*, 2005). Crystals were subsequently grown by sitting drop vapor diffusion, adding 1 μl of 1.4 M sodium acetate, 0.1 M sodium cacodylate, pH 6.5–1 μl of protein solution at 10 mg/ml. The crystals were cryoprotected with 25% ethylene glycol. Heavy-atom derivatives for isomorphous replacement were prepared by soaking crystals overnight in pre-equilibrated

Table I Crystallographic data

Crystal	λ (Å)	Resolution (Å)	$I/\sigma I$[a]	Rm[b] (%)	Multiplicity[c]	Completeness (%)[d]
NATI	0.931	2.8	23.3 (5.3)	0.078 (0.456)	11.6 (12.0)	99.9 (99.9)
Ru	0.931	3.2	38.5 (11.6)	0.107 (0.377)	40.3 (41.3)	99.9 (99.9)
Pt	0.931	3.2	31.7 (13.3)	0.094 (0.242)	22.9 (23.8)	99.8 (99.8)
Au	0.931	3.2	19.2 (3.0)	0.114 (0.372)	12.7 (6.4)	97.6 (84.7)
Os	0.931	3.2	24.8 (11.6)	0.069 (0.173)	9.7 (10.1)	99.9 (99.9)

Escherichia coli plasmid pB171 ParR (NP_053129, pB171_067, 1–130 full length, no tag) P6(1)22, $a = b = 96.8$ Å, $c = 124.9$ Å.
[a]Signal to noise ratio for merged intensities.
[b]Rm: $\Sigma h \Sigma i |I(h,i) - I(h)| / \Sigma h \Sigma i\, I(h,i)$ where $I(h,i)$ are symmetry-related intensities and $I(h)$ is the mean intensity of the reflection with unique index h.
[c]Multiplicity for unique reflections.
[d]Completeness for unique reflections. Highest resolution bins in brackets. The final figure of merit, after phasing with SHARP, was 0.46–3.1 Å resolution using the four derivatives.

Table II Refinement statistics

Model	2 monomers/ASU 2 chains A & B Residues 6–95 ordered (1–130 full-length crystallized) 26 water molecules
Diffraction data	NATI, 30.7–2.8 Å, all data
R-factor, R-free[a]	0.24 (0.38), 0.28 (0.45)
B-factors[b]	54.9 Å^2, 1.74 Å^2
Geometry[c]	0.007 Å, 1.35°
Ramachandran[d]	90.0%/0.0%
NCS (unrestrained)[e]	2.08 Å
PDB ID	2JD3

[a]5% of reflections were randomly selected for determination of the free R-factor, before any refinement. R-factors for the highest resolution bins are given in brackets.
[b]Temperature factors averaged for all atoms and RMS deviation of temperature factors between bonded atoms.
[c]RMS deviations from ideal geometry for bond lengths and restraint angles.
[d]Percentage of residues in the 'most favored region' of the Ramachandran plot and percentage of outliers.
[e]NCS: 'no noncrystallographic restraints (NCS)' were used during refinement because of significant differences between chain A and chain B, most notably in the C-terminus. The number in the table gives the RMSD of all atoms present in both chains A and B.

drops containing K_2RuCl_6, K_2PtCl_6, $K_2Au(CN)_2$ and K_2OsCl_6 (Table I). Diffraction data for native (NATI) and derivatized crystals were collected on beamline ID14eh4 (ESRF, Grenoble, France). Crystallographic data are presented in Table I. The structure of pB171 ParR was solved by isomorphous replacement. Initial sites were found using SHELXDE (Uson and Sheldrick, 1999) and refined with SHARP (de La Fortelle and Bricogne, 1997) and marginal sites were added. The final figure of merit using four derivates was 0.46 up to 3.1 Å resolution. After density modification, the density was of very good quality and could be built in one session. Refinement was performed using CNS 1.1 (Brunger *et al*, 1998). Refinement statistics are presented in Table II. The coordinates have been deposited in the Protein Data Bank with accession code 2jd3.

Electron microscopy

Negatively stained samples were prepared on glow-discharged carbon-coated grids according to a modified deep stain protocol (Stoops *et al*, 1992). Briefly, a 383 bp PCR product encoding the *parC* region was constructed using the primers: SR14: GCGAAA GGGGGATGTGCTGC; SR15: CCCAGGCTTTACACTTTATGC with pMD330 (Dam and Gerdes, 1994) as template and the PCR product was purified using a Qiaquick PCR-purification kit. Standard reactions for negative stain were performed in a total volume of 15 µl 20 mM Tris pH 7.5, 50 mM KCl, 2 mM $MgCl_2$. *parC* DNA was added to a final concentration of 10 ng/µl and R1 ParR was added to a concentration of 1 µM. The samples were incubated 15 min at room temperature and diluted fivefold in buffer. Samples (3 µl) were loaded on glow-discharged carbon-coated grids. After 30 s, grids were rinsed with 2% uranyl acetate, blotted dry with filter paper, and further dried with a hairdryer.

Rotary-shadowed samples were prepared on glow-discharged carbon-coated grids essentially as described by Williams (1977). pMD330 (Dam and Gerdes, 1994) was linearized by *Sca*I (NEB) cleavage for 5 h at 37°C and purified with a Qiaquick PCR-purification kit. Standard reactions for rotary shadowing were performed in a total volume of 15 µl 20 mM Tris pH 7.5, 50 mM KCl, 2 mM $MgCl_2$. Linearized pMD330 was added to a final concentration of 1 ng/µl and R1 ParR was added to a final concentration of 500 nM. Reactions were incubated 15 min at room temperature and a 3 µl sample was loaded on a glow-discharged carbon-coated grid. After 30 s, grids were rinsed with 0.05% uranyl acetate, blotted with filter paper and dried in a stream of air. Rotary shadowing was performed in an Edwards E306A coating system by using a platinum source with an oblique angle of 6° and a sample-to-source distance of 8 cm.

Electron microscopy was performed at 80 kV using a Philips EM208 transmission electron microscope. Images were photographed at a magnification of ×32–40 k and negatives were scanned at 6 µm/pixel using a MRC-KZA scanner.

Determination of plasmid stability

Plasmid loss curves were determined as described by Gerdes *et al* (1985). *E. coli* DH5α cells were grown in nonselective medium and the fraction of plasmid-bearing cells was determined by plating on nonselective indicator plates containing X-gal. As the β-galactosidase gene is located on the plasmid in these strains, the plasmid content can be determined by scoring blue and white colonies.

Electrophoretic mobility shift assay

Gelshift analysis was carried out essentially as described by Ringgaard *et al* (2007). Briefly, 354 bp *parC* DNA fragments obtained by PCR using primers 5′-GTATACGTTCATCTATAGCCC, 5′-GATCTCCGTTTAACAGGCAG and pGE3 (Ebersbach and Gerdes, 2001) as template. Control fragments of 318 bp were generated from pUC19 DNA using primers 5′-CGACAGGTTTCCCGACTGG, and 5′-CAGCTGGCGAAAGGGGGATG. DNA fragments were end-labeled with ^{32}P and purified from a 1% agarose gel. The binding reaction contained 2 nM ^{32}P-labeled DNA in 10 mM Tris–HCl pH 7.5, 50 mM KCl, 50 mM NaCl, 1 mM $MgCl_2$, 0.5 mM DTT, 0.5 mM EDTA, 0.1 mg/ml BSA and 0.1 mg/ml sonicated salmon sperm competitor DNA. Two micromolar wt or mutant ParR171 was added and the reactions were incubated for 30 min at 25°C. Following addition of glycerol to a concentration of 3%, the samples were loaded on a 5% polyacrylamide gel.

Fluorescence anisotropy

Fluorescence anisotropy was recorded at 298 K using a Perkin-Elmer LS55 luminescence spectrometer. An 88-bp fluorescein-labeled PCR product containing the *parC1* region from plasmid pB171 was generated using primers JMJ32 (5′-GATAGTGCTCAAATTGAGTATT ACC-3′) and JMJ33 (5′-GTATACGTTCATCTATAGCCCC-3′) and used at a concentration of 2 nM for binding reactions. Wt and mutant ParR171 protein was serially titrated into the cuvette at concentrations ranging from 0–5 µM in binding buffer (20 mM Tris–HCl pH 8.8; 25 mM NaCl; 1 mM DTT; 1 mM EDTA) and allowed to equilibrate for 2 min before measurement.

Acknowledgements

We gratefully acknowledge support from the staff at beamline ID14eh4 at the ESRF (Grenoble, France). JMJ was supported by fellowships from EMBO and the Danish Research Council.

References

Barilla D, Rosenberg MF, Nobbmann U, Hayes F (2005) Bacterial DNA segregation dynamics mediated by the polymerizing protein ParF. *EMBO J* **24:** 1453–1464

Becker E, Herrera NC, Gunderson FQ, Derman AI, Dance AL, Sims J, Larsen RA, Pogliano J (2006) DNA segregation by the bacterial actin AlfA during *Bacillus subtilis* growth and development. *EMBO J* **25:** 5919–5931

Bouet JY, Ah-Seng Y, Benmeradi N, Lane D (2007) Polymerization of SopA partition ATPase: regulation by DNA binding and SopB. *Mol Microbiol* **63:** 468–481

Bouet JY, Surtees JA, Funnell BE (2000) Stoichiometry of P1 plasmid partition complexes. *J Biol Chem* **275:** 8213–8219

Brunger AT, Adams PD, Clore GM, DeLano WL, Gros P, Grosse-Kunstleve RW, Jiang JS, Kuszewski J, Nilges M, Pannu NS, Read RJ, Rice LM, Simonson T, Warren GL (1998) Crystallography & NMR system: a new software suite for macromolecular structure determination. *Acta Crystallogr D* **54:** 905–921

Dam M, Gerdes K (1994) Partitioning of plasmid R1. Ten direct repeats flanking the parA promoter constitute a centromere-like partition site parC, that expresses incompatibility. *J Mol Biol* **236:** 1289–1298

de La Fortelle E, Bricogne G (1997) Maximum-likelihood heavy-atom parameter refinement for the multiple isomorphous replacement and multiwavelength anomalous diffraction methods. *Methods in Enzymology* **276:** 472–494

Ebersbach G, Gerdes K (2001) The double par locus of virulence factor pB171: DNA segregation is correlated with oscillation of ParA. *Proc Natl Acad Sci USA* **98:** 15078–15083

Ebersbach G, Ringgaard S, Møller-Jensen J, Wang Q, Sherratt DJ, Gerdes K (2006) Regular cellular distribution of plasmids by oscillating and filament-forming ParA ATPase of plasmid pB171. *Mol Microbiol* **61:** 1428–1442

Edgar R, Chattoraj DK, Yarmolinsky M (2001) Pairing of P1 plasmid partition sites by ParB. *Mol Microbiol* **42:** 1363–1370

Errington J, Murray H, Wu LJ (2005) Diversity and redundancy in bacterial chromosome segregation mechanisms. *Philos Trans R Soc Lond B Biol Sci* **360:** 497–505

Fogel MA, Waldor MK (2006) A dynamic, mitotic-like mechanism for bacterial chromosome segregation. *Genes Dev* **20:** 3269–3282

Garner EC, Campbell CS, Mullins RD (2004) Dynamic instability in a DNA-segregating prokaryotic actin homolog. *Science* **306:** 1021–1025

Garner EC, Campbell CS, Weibel DB, Mullins RD (2007) Reconstitution of DNA segregation driven by assembly of a prokaryotic actin homolog. *Science* **315:** 1270–1274

Gerdes K, Larsen JE, Molin S (1985) Stable inheritance of plasmid R1 requires two different loci. *J Bacteriol* **161:** 292–298

Gerdes K, Møller-Jensen J, Bugge JR (2000) Plasmid and chromosome partitioning: surprises from phylogeny. *Mol Microbiol* **37:** 455–466

Gerdes K, Møller-Jensen J, Ebersbach G, Kruse T, Nordstrom K (2004) Bacterial mitotic machineries. *Cell* **116:** 359–366

Golovanov AP, Barilla D, Golovanova M, Hayes F, Lian LY (2003) ParG, a protein required for active partition of bacterial plasmids, has a dimeric ribbon–helix–helix structure. *Mol Microbiol* **50:** 1141–1153

Gomis-Ruth FX, Sola M, Acebo P, Parraga A, Guasch A, Eritja R, Gonzalez A, Espinosa M, del SG, Coll M (1998) The structure of plasmid-encoded transcriptional repressor CopG unliganded and bound to its operator. *EMBO J* **17:** 7404–7415

Hayes F (2000) The partition system of multidrug resistance plasmid TP228 includes a novel protein that epitomizes an evolutionarily distinct subgroup of the ParA superfamily. *Mol Microbiol* **37:** 528–541

Hoischen C, Bolshoy A, Gerdes K, Diekmann S (2004) Centromere parC of plasmid R1 is curved. *Nucleic Acids Res* **32:** 5907–5915

Jensen RB, Dam M, Gerdes K (1994) Partitioning of plasmid R1. The parA operon is autoregulated by ParR and its transcription is highly stimulated by a downstream activating element. *J Mol Biol* **236:** 1299–1309

Jensen RB, Lurz R, Gerdes K (1998) Mechanism of DNA segregation in prokaryotes: replicon pairing by parC of plasmid R1. *Proc Natl Acad Sci USA* **95:** 8550–8555

Lee PS, Grossman AD (2006) The chromosome partitioning proteins Soj (ParA) and Spo0J (ParB) contribute to accurate chromosome partitioning, separation of replicated sister origins, and regulation of replication initiation in *Bacillus subtilis*. *Mol Microbiol* **60:** 853–869

Leonard TA, Butler PJ, Löwe J (2005) Bacterial chromosome segregation: structure and DNA binding of the Soj dimmer—a conserved biological switch. *EMBO J* **24:** 270–282

Lim GE, Derman AI, Pogliano J (2005) Bacterial DNA segregation by dynamic SopA polymers. *Proc Natl Acad Sci USA* **102:** 17658–17663

Møller-Jensen J, Borch J, Dam M, Jensen RB, Roepstorff P, Gerdes K (2003) Bacterial mitosis: ParM of plasmid R1 moves plasmid DNA by an actin-like insertional polymerization mechanism. *Mol Cell* **12:** 1477–1487

Møller-Jensen J, Jensen RB, Löwe J, Gerdes K (2002) Prokaryotic DNA segregation by an actin-like filament. *EMBO J* **21:** 3119–3127

Raumann BE, Brown BM, Sauer RT (1994a) Major groove DNA recognition by beta-sheets: the ribbon–helix–helix family of gene regulatory proteins. *Curr Opin Struct Biol* **4:** 36–43

Raumann BE, Rould MA, Pabo CO, Sauer RT (1994b) DNA recognition by beta-sheets in the Arc repressor-operator crystal structure. *Nature* **367:** 754–757

Ringgaard S, Ebersbach G, Borch J, Gerdes K (2007) Regulatory cross-talk in the double par locus of plasmid pB171. *J Biol Chem* **282:** 3134–3145

Schumacher MA, Funnell BE (2005) Structures of ParB bound to DNA reveal mechanism of partition complex formation. *Nature* **438:** 516–519

Somers WS, Phillips SE (1992) Crystal structure of the met repressor-operator complex at 2.8 Å resolution reveals DNA recognition by beta-strands. *Nature* **359:** 387–393

Stock D, Perisic O, Löwe J (2005) Robotic nanolitre protein crystallisation at the MRC laboratory of molecular biology. *Prog Biophys Mol Biol* **88:** 311–327

Stoops JK, Kolodziej SJ, Schroeter JP, Bretaudiere JP, Wakil SJ (1992) Structure–function relationships of the yeast fatty acid synthase: negative-stain, cryo-electron microscopy, and image analysis studies of the end views of the structure. *Proc Natl Acad Sci USA* **89:** 6585–6589

Uson I, Sheldrick GM (1999) Advances in direct methods for protein crystallography. *Curr Opin Struct Biol* **9:** 643–648

van den Ent F, Löwe J (2000) Crystal structure of the cell division protein FtsA from Thermotoga maritima. *EMBO J* **19:** 5300–5307

van den Ent F, Møller-Jensen J, Amos LA, Gerdes K, Löwe J (2002) F-actin-like filaments formed by plasmid segregation protein ParM. *EMBO J* **21:** 6935–6943

Weihofen WA, Cicek A, Pratto F, Alonso JC, Saenger W (2006) Structures of omega repressors bound to direct and inverted DNA repeats explain modulation of transcription. *Nucleic Acids Res* **34:** 1450–1458

Williams RC (1977) Use of polylysine for adsorption of nuclei acids and enzymes to electron microscope specimen films. *Proc Natl Acad Sci USA* **74:** 2311–2315

Wu LJ, Errington J (2003) RacA and the Soj-Spo0J system combine to effect polar chromosome segregation in sporulating *Bacillus subtilis*. *Mol Microbiol* **49:** 1463–1475

Yamaichi Y, Fogel MA, Waldor MK (2007) Par genes and the pathology of chromosome loss in *Vibrio cholerae*. *Proc Natl Acad Sci USA* **104:** 630–635

Yamaichi Y, Niki H (2000) Active segregation by the *Bacillus subtilis* partitioning system in *Escherichia coli*. *Proc Natl Acad Sci USA* **97:** 14656–14661

